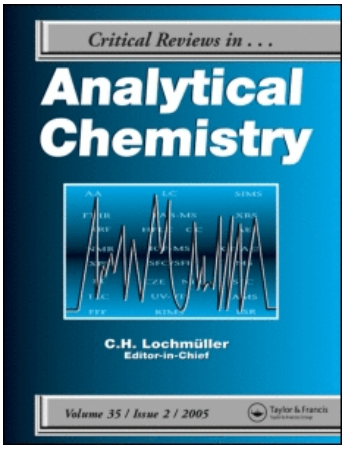

Critical Reviews in Analytical Chemistry
Publication details, including instructions for authors and subscription information:
http://www.informaworld.com/smpp/title~content=t713400837

Infrared Spectroscopy in Electrochemistry: New Methods and Connections to UhV Surface Science

Carol Korzeniewski[a]
[a] Department of Chemistry and Biochemistry, Texas Tech University, Lubbock, TX

To cite this Article Korzeniewski, Carol(1997) 'Infrared Spectroscopy in Electrochemistry: New Methods and Connections to UhV Surface Science', Critical Reviews in Analytical Chemistry, 27: 2, 81 — 102
To link to this Article: DOI: 10.1080/10408349708050584
URL: http://dx.doi.org/10.1080/10408349708050584

Critical Reviews in Analytical Chemistry, 27(2):81–102 (1997)

Infrared Spectroscopy in Electrochemistry: New Methods and Connections to UhV Surface Science

*Carol Korzeniewski**

Department of Chemistry and Biochemistry, Texas Tech University, Lubbock, TX 79409–1061

* Phone: 806/742-3059; Fax: 806/742-1289; email: bfkor@ttacs.ttu.edu

ABSTRACT: This review discusses recent advances in the use of infrared spectroscopy in electrochemistry. The central focus is on analytical factors that affect the ability to derive structural information from infrared spectra of molecular adlayers. The effects of vibrational coupling and dielectric screening are emphasized. Applications of real-time polarization modulation and step-scan Fourier transform infrared spectroscopy are also presented.

KEY WORDS: infrared spectroscopy, electrochemistry, surface chemistry, single crystal electrodes, vibrational coupling.

I. INTRODUCTION

Infrared spectroscopy has been used widely in electrochemistry. Spectra aid the identification of reactants, products, and long-lived intermediates and allow potential dependent changes in the interfacial solvent and electrolyte composition to be tracked. A variety of spectral sampling and data acquisition methods have been developed to approach *in situ* detection of species ranging from submonolayers on low surface area single crystals[1–3] to solution phase products of fuel cell reactions.[4]

Reviews of infrared spectroscopy in electrochemistry have appeared since the mid-1980s.[1–3,5–17] The common data acquisition and spectral sampling techniques have been described. Therefore, the methods and instrumentation are mentioned but not discussed in detail here. This review focuses mainly on the delineation of adlayer structural characteristics from infrared spectra and briefly describes new developments in the use of polarization modulation techniques and step-scan Fourier transform infrared spectroscopy (FTIR). Connections between the infrared spectra and atomic level structure of molecular adlayers are highlighted for systems where the adlayer structures are available from *in situ* scanning tunneling microscopy (STM). The analytical importance of vibrational coupling and dielectric screening are discussed in conjunction with infrared spectra of well-defined, *in situ* STM-characterized adlayers on (111) surface planes and more complicated adlayer structures on stepped surfaces. The review concludes with short accounts of the real-time sampling electronics for polarization modula-

1040-8347/97/$.50

tion spectroscopy, recent applications of real-time polarization modulation in electrochemistry, and advances in electrochemically modulated step-scan FTIR spectroscopy.

II. EXPERIMENTAL

A. Sampling Methods

External reflection sampling methods are typically used to obtain *in situ* infrared spectra of species generated electrochemically (Figure 1). In this arrangement, the infrared beam is directed through a polarizer and onto the front surface of a highly polished disk-shaped working electrode. A special thin-layer electrochemical cell is employed that permits the infrared beam to enter and strike the front surface of the polished disk at an incidence angle of about 60° to 70° with respect to the surface normal. From the surface of the working electrode the beam is reflected out of the cell and is collected by optics that image the radiation onto a detector. This arrangement requires the use of electrode materials that have high reflectivities in the infrared spectral region. Platinum, gold, and silver have been employed most frequently.

The simple optical layout in Figure 1A has been used for static linear polarization (SLP) experiments. The polarizer is set to allow radiation with its electric field vector oriented parallel to the plane of incidence (p-polarized radiation) to strike the electrode surface.[5–7,11,18–23] Interference between the incident and reflected beams creates a standing electromagnetic wave at the metal surface. The electric field intensity at the surface is influenced by interactions with the image dipole in the metal and reaches a maximum when p-polarized light strikes at high angles of incidence (cf. References 11,18–20). Maximum detectability of adsorbates and species in the diffuse double layer is achieved under these conditions. The component of the radiation-polarized perpendicular to the plane of incidence (s-polarized radiation) undergoes a phase shift of about 180° at the electrode surface for all angles of incidence. Hence, the amplitude of the electric field for the s-polarized radiation is near zero at the metal surface.

The optical configuration shown in Figure 1B has been used recently for external reflection polarization modulation experiments with an FTIR spectrometer.[24–26] This layout includes a photoelastic modulator (PEM), which rapidly (74 kHz) switches the polarization state of the radiation, reaching the electrode between parallel and perpendicular. Demodulation of the detector signal gives a difference waveform that carries spectral information about species that respond differently to the surface-sensitive (p) and surface-insensitive (s) polarization components. This technique effectively discriminates against interferences that are insensitive to the polarization state of the radiation beam, such as instrument drift and atmospheric water vapor and CO_2.[5–7] It has advanced recently with the development of high-speed digital electronics for signal demodulation and the use of an infrared lens in place of a detector-focusing mirror to reduce polarization phase shifts after the electrode.[24–26] Polarization modulation is discussed in greater detail in Sections II.C and III.B.

Attenuated total internal reflection (ATR) sampling methods have also been used to obtain *in situ* infrared spectra of electrochemical species.[12,27–30] Figure 2 shows a recent cell design. The working electrode is a thin film of metal deposited onto one surface of an ATR crystal. The metal film must be sufficiently thin to allow penetration of the infrared evanescent wave[31] beyond the metal-solution interface. For the cell in Figure 2, the ATR crystal forms the bottom of a chamber that holds the electrolyte solution and the counter and reference electrodes. The crystal is positioned so that the metal film is inside the chamber. Special optics

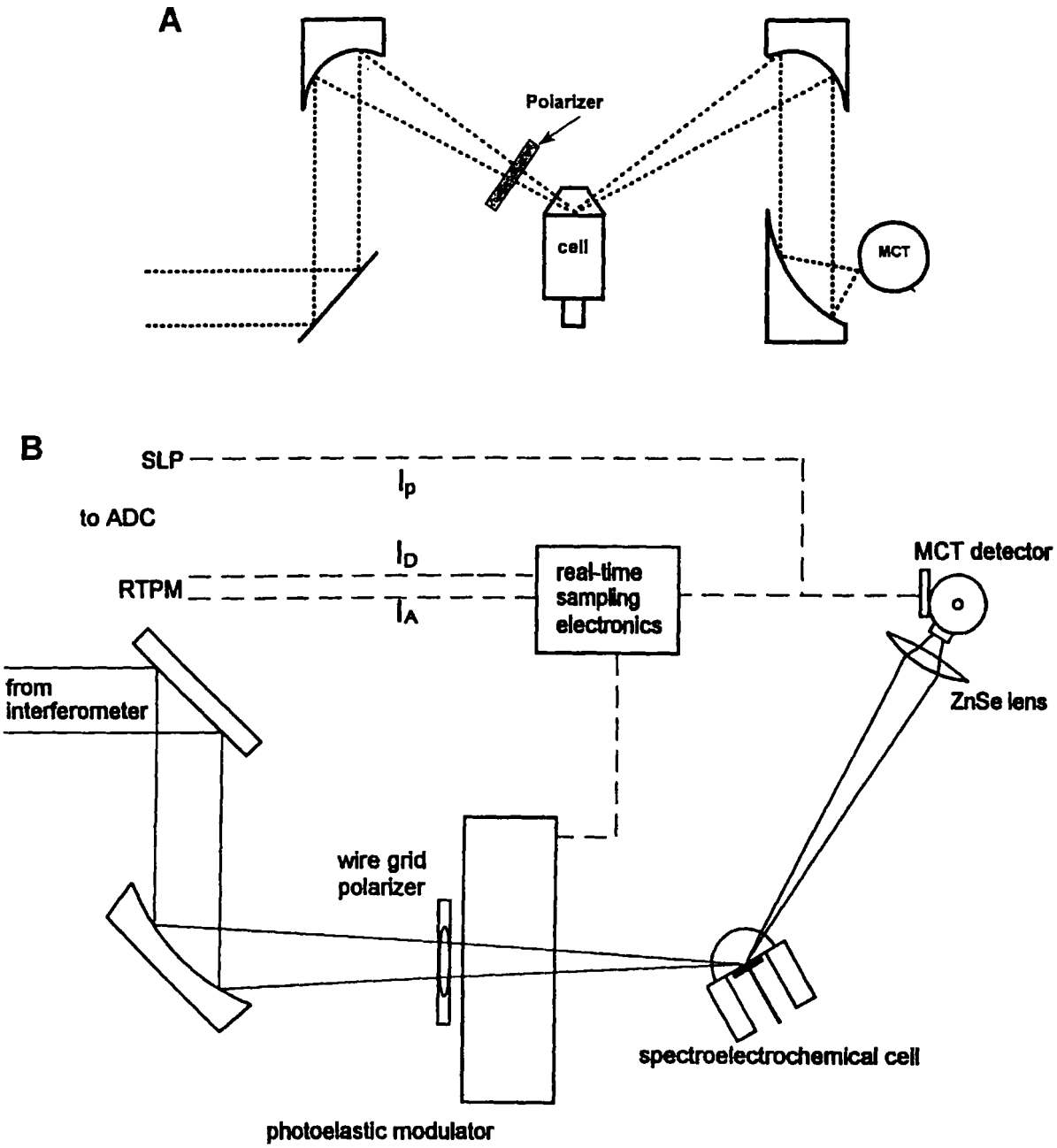

FIGURE 1. External reflection optical configurations for infrared spectroelectrochemistry. (A) Symmetrical arrangement based on 6.9-in focal length, 60° off-axis parabolic mirrors. (B) Optical layout and electronic configuration for polarization modulation experiments. See text for abbreviations. (Part B reprinted from Reference 24 with permission.)

direct infrared radiation into the crystal and capture the radiation as it exits.

ATR sampling has not been used widely in electrochemistry. Preparation and use of the thin metal film working electrodes has been difficult. Nevertheless, this technique has been pursued because it can overcome molecular transport limitations imposed by external reflection methods. Formation of a thin (~1 to 5 μm) solution layer between the

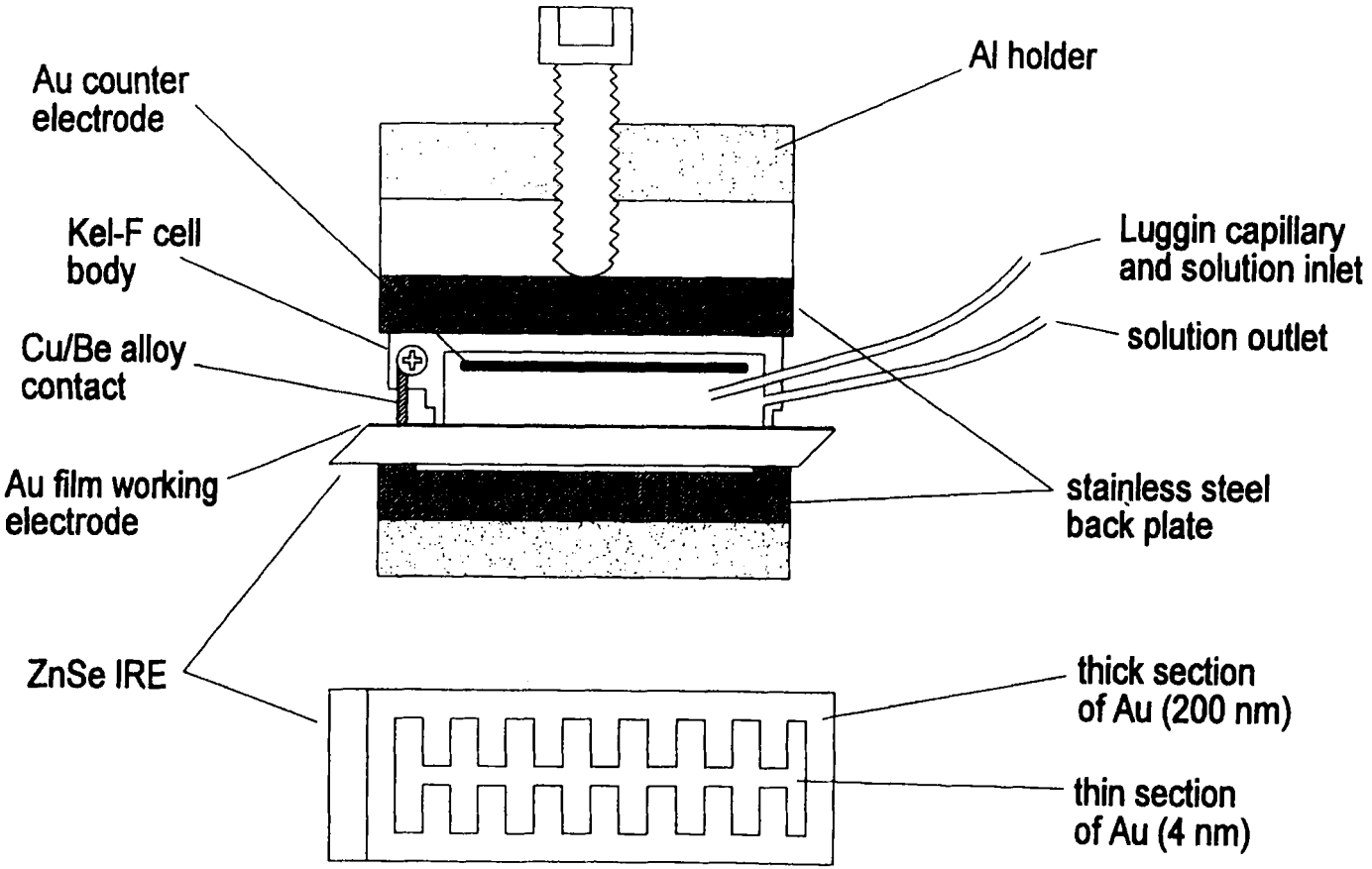

FIGURE 2. Electrochemical cell for *in situ* ATR infrared spectroscopy sampling. A top view of the patterned working electrode/internal reflection element is shown in the bottom of the figure. The numbers in parentheses are the thicknesses of the gold deposits in the two sections. (Reprinted from Reference 27 with permission.)

front face of the working electrode and the infrared transparent window is required for external reflection experiments (see Section II.B) to minimize absorption of infrared radiation by the solvent. However, diffusion of species into and out of the thin layer region is restricted and can lead to reactant depletion, product accumulation, and changes in the pH and ionic composition of the cavity.[32-36] Increased solution resistance in the thin layer can also limit potential control. Because a thin layer is not required for ATR experiments, more favorable electrode arrangements can be used.

The ATR method suffers most from the stability and transparency of the metal film working electrode. With improvements in the working electrode, the ATR technique will be used more widely in electrochemistry. All of the applications presented in this review involve the use of external reflection sampling.

B. Thin-Layer Electrochemical Cells

Thin-layer electrochemical cells for external reflection infrared spectroscopy have been described by several authors.[5,8,9,11,37-39] Specific design features are not discussed in depth in this review. More recently, work has focused on understanding how detection is affected by the physical and optical characteristics of the thin layer cavity. Studies in this area are highlighted.

Figure 3 shows a drawing of a typical cell. The working electrode is a metal disk approximately 6 to 10 mm in diameter. The front face of the disk is polished to a mirror finish, typically with a slurry of alumina or diamond paste. The disk is mounted in a plunger and the sides are sealed to prevent contact with the electrolyte solution. Electrical contact to the disk is made through a wire spot-welded to the back. The counter electrode is typically platinum wire or gauze that is looped around the working electrode plunger and positioned just behind the metal disk. The reference electrode mounts in an external compartment that connects to the main chamber through a Luggin capillary.

An infrared transparent window attaches to the front of the cell. The working electrode is positioned so that the polished front face is adjacent to the optically flat surface of the window. During infrared spectroscopy experiments, the electrode is pushed against the window and a thin (ca. 1 to 5 μm) solution layer becomes entrapped (Figure 3, expanded view). The thin layer allows infrared radiation to reach the reflective surface of the working electrode with minimal attenuation by the solvent.

The optical properties of the thin layer affect the sensitivity of infrared measurements. The thickness of this region can be smaller than the wavelengths of radiation in the mid-infrared range, and because p- and s-polarizations have different electric field amplitudes at the electrode surface, the spatial distribution of these waves in the cavity is inhomogeneous.[37,38] The spatial properties of the electromagnetic field depend on the optical constants of the metal, the solution layer, the adsorbate layer and the window, and on the angle of incidence and polarization state of the infrared beam.[37,38,40-43] In general, high incidence angles and parallel polarized radiation are required in order to maintain an appreciable electric field at the metal surface, but the preferred optical geometry depends on the specific system under study. Important work has defined experimental conditions for maximum detectability of interfacial species by applying classic electromagnetic theory to determine how the optical properties of the complete electrochemical system influence reflectance spectra.[37-44] The reflection and throughput characteristics of the cell can be improved by using trapezoidal[37,40,42] (Figure 3) or hemispherical (Figure 1B)[38,39,44] windows that allow normal incidence at the air/window interface.

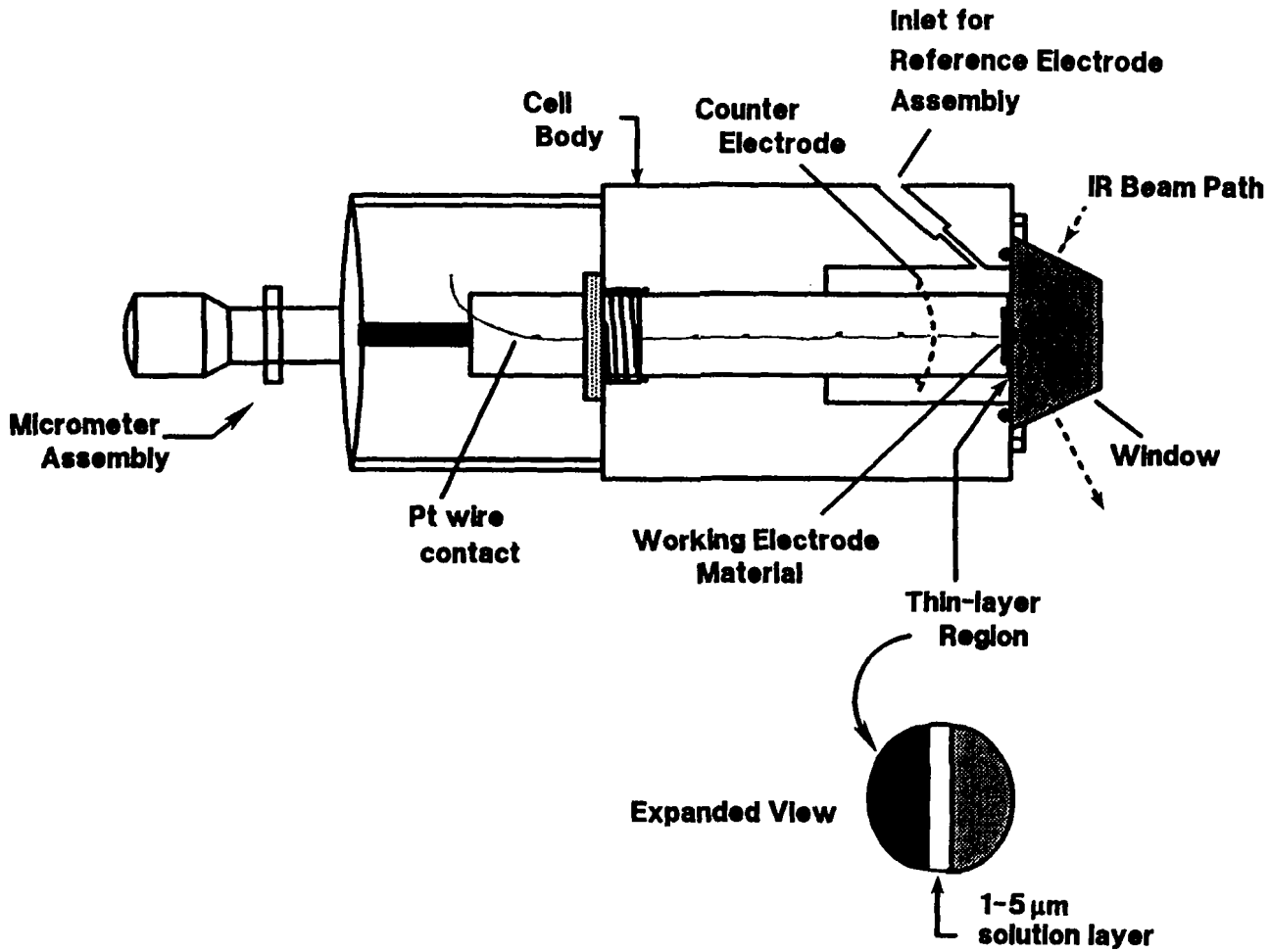

FIGURE 3. Schematic diagram of an electrochemical cell designed for *in situ* infrared spectroscopy measurements via external reflection sampling. A slice through the center of the cell viewed from the top is shown. An expanded view of the thin layer cavity region also appears. (Reprinted from Reference 3, with kind permission of Elsevier Science, The Netherlands.)

C. Spectral Acquisition

Acquisition of *in situ* infrared spectra has been achieved by several methods. Potential difference techniques reduce background solvent absorption and have been most widely applied. The simplest approach involves the use of a FTIR spectrometer and static linear polarization. A sequence of interferograms is collected while the electrode is held at a constant potential. The interferograms are coadded, averaged, Fourier transformed to a single beam spectrum, and electronically stored. The electrode is then stepped to a new potential, the data collection and processing is repeated, and the resulting single beam spectrum is stored in a new file. The single beam spectra encode the wavelength dependent reflectivity of the system, $R(\lambda)$. A potential difference spectrum is computed from the ratio of single beam spectra recorded at two different electrode potentials. Spectra are typically displayed as either $(R_2(\lambda)/R_1(\lambda) - 1) \equiv \Delta R/R$, or as $-\log(R_2(\lambda)/R_1(\lambda))$, where the subscripts signify the two potentials.

The method described above involving the sequential acquisition of interferograms has sometimes been referred to as single potential alteration infrared spectroscopy (SPAIRS).[45,46] It is one of the "SNIFTIRS" (subtractively normalized interfacial Fourier transform infrared spectroscopy) techniques; SNIFTIRS encompasses a group of methods that utilize a FTIR spectrometer and static linear polarization (cf. References 5 to 7). An alternative to SPAIRS is potential modulation SNIFTIRS, in which the electrode potential is modulated between two values while a small number of interferograms is collected at each value. Interferograms recorded at the same potential are coadded, and at the end of data acquisition the two interferogram files are Fourier transformed and stored. Potential difference spectra are computed from the two single beam spectra as described above. Potential modulation improves the spectral signal-to-noise ratio by compensating for instrument drift and infrared absorption by atmospheric CO_2 and water vapor. However, it is only appropriate for use in cases where the systems under study display reversible electrochemistry. Electrochemically modulated infrared spectroscopy (EMIRS) is a related technique that employs a dispersive infrared spectrometer instead of an FTIR spectrometer.[5,6,47] The first *in situ* infrared spectra of electrochemical species were obtained with EMIRS (cf. References 5,6,47). With EMIRS, the potential is modulated at about 10 Hz as the monochrometer is slowly scanned. A differential spectral signal is recovered with phase-sensitive detection.

In situ spectra are also recorded with polarization modulation techniques.[5,6,9,24,48–54] Like potential modulation, polarization modulation minimizes disturbances from instrument drift and atmospheric gases. In these experiments, differential reflectance ($\Delta R/R$) spectra are computed as the ratio of $(I_s - I_p)/(I_s + I_p)$, where I_p is the intensity of reflected p-polarized radiation and I_s is the intensity of reflected s-polarized radiation. The sum $((I_s + I_p))$ and difference $((I_s - I_p))$ spectra are derived by Fourier transformation of the interferogram signal before and after demodulation, respectively. With polarization modulation, it is possible to record an *in situ* infrared spectrum of an electrode at a single potential. However, because s- and p-polarized radiation do not sample equivalent regions of the thin solution layer between the working electrode and the window, the differential (demodulated) spectral signal contains a strong background from the bulk solvent and electrolyte. In addition, the PEM has a wavelength dependence that adds a slowly varying sinusoidal component to the differential reflectance spectra.[25,26] Therefore, polarization modulation spectra recorded at two different electrode potentials are typically ratioed to eliminate the bulk features and correct the spectral baseline.[5,6,24,49–53,55]

D. Surface Selection Rule

Due to the image dipole effects discussed in Section II.A, infrared electromagnetic fields at the surface of a metal are preferentially oriented normal to the surface.[5,6,11,19–23] The surface-induced polarization of the infrared radiation limits the detectable vibrational modes of adsorbed molecules to those with a component of their transition dipole moment normal to the surface. Transition dipole moments oriented parallel to the surface cannot be excited. This property is known as the "surface selection rule" and provides information about the orientation of adsorbed molecules.[5,6,11,18–23]

III. APPLICATIONS AND RECENT EXPERIMENTAL DEVELOPMENTS

A. Adsorption on Single Crystal Electrodes: Relationships among Infrared Spectra and Adsorbate Structure, Coverage, and Site-Occupancy

Infrared spectroscopy is applied most often in electrochemistry to study reactions and adsorption at conventional polycrystalline working electrodes. Its use in single crystal electrochemistry has become possible with the development of bench-top methods for cleaning and ordering single crystal surfaces.[56–64] Atomically well-defined materials have enabled the study of surface geometric and electronic influences on processes such as electrocatalytic reactions, electrodeposition, and the assembly of organic monolayers.[2,3,11,65,66] In support of this work, infrared spectroscopy has been used to identify reactants, products, and adlayer structural characteristics and to track charge compensating ions.[2,3,11,17,24,65–67]

Some important advances in the use of infrared spectroscopy in electrochemistry have occurred through the study of small organic molecule oxidation reactions on single crystal electrodes.[3,14,65] Many of these reactions progress through adsorbed carbon monoxide (CO). This adsorbate has a strong C-O stretching transition dipole moment and has been detected on electrodes at coverages down to 1/10 of a monolayer.[2,68–70] The frequencies and intensities of the C-O stretching vibrational bands are sensitive to the two-dimensional arrangement of the adsorbed molecules. At low and intermediate coverages, infrared spectra have been used to determine if the CO adlayer forms as dense islands or more dispersed assemblies.[3,68] These studies have been aided by structural information derived from vibrational spectra of CO adlayers on single crystal metals in ultra high vacuum (uhv).[2,17,68,69,71] Work in this area has been reviewed recently.[3]

Closer relationships between *in situ* infrared spectra of adsorbates and specific adlayer structures have been derived through the use of *in situ* STM.[17,72–77] Challenges associated with *in situ* STM have limited detailed comparisons to adsorbed CO. However, a wealth of information has been obtained regarding the chemical and physical properties of CO adlayers on platinum-group transition metals. Some developments in the use of *in situ* STM are described in Section III.A.1, and issues related to infrared spectral analysis are presented in Sections III.A.2 and III.A.3.

Another area of interest has been on site-dependent adsorption at stable high index surface planes of single crystal electrodes. These surfaces have well-defined step and kink sites that serve as models of the defects and edges on practical catalysts. Experiments with stepped single crystal electrodes have identified factors that limit infrared spectroscopic detection of molecules at different structural sites. Recent work in this area is discussed in Section III.A.4.

The influence of dielectric screening on *in situ* infrared spectra of species adsorbed

on electrodes was uncovered recently in uhv experiments that simulated solvation at electrochemical interfaces.[17,78] A reduction in vibrational band intensity results when solvent and other polarizable species surrounding an adsorbate screen the adsorbate transition dipole moments. Dielectric screening and its consequences are considered in Section III.A.5.

1. Adlayer Structure Probed by In situ STM and Infrared Spectroscopy

Figure 4 shows infrared spectra of CO adsorbed at saturation coverages on Pt(111) at –0.25 V and +0.1 V (vs. a saturated calomel reference electrode (SCE)).[72] The spectra were obtained by using the SPAIRS technique. The background single beam spectrum was obtained at a potential, +0.5 V, where the surface is free of adsorbed CO due to its oxidation to CO_2. The strong band that extends downward near 2345 cm^{-1} in each spectrum results from CO_2 formation at the background potential.

The vibrational bands that arise from the CO monolayer at the indicated potentials extend upward in Figure 4. The strong bands at 2073 cm^{-1} and 2066 cm^{-1} fall in the range of the C-O stretching modes for atop coordinated CO (i.e., CO bonded to a single sur-

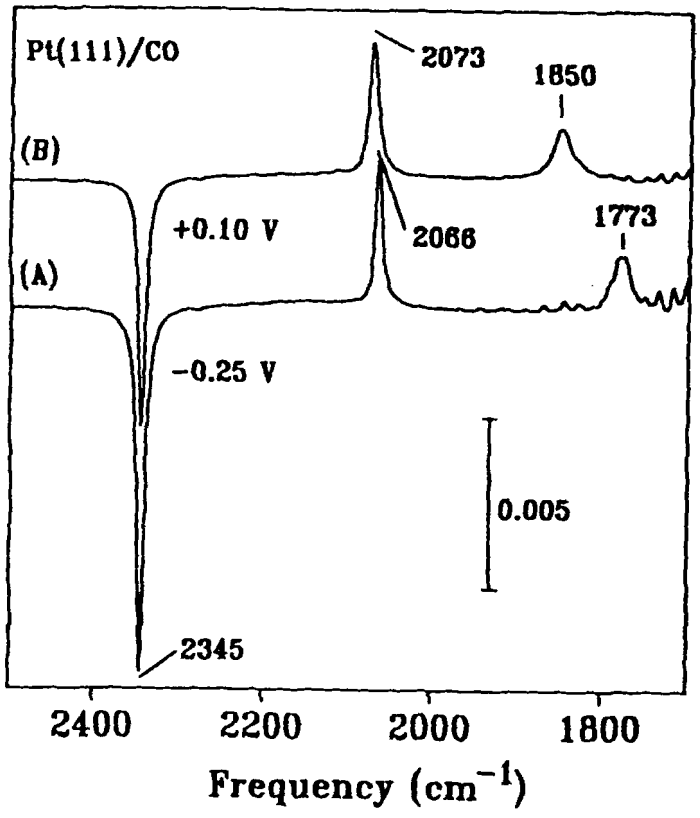

FIGURE 4. Infrared spectra of a Pt(111) electrode in CO saturated 0.1 M $HClO_4$ solution. The electrode potential is (A) –0.25 V and (B) +0.10 V vs. SCE. The reference spectrum was acquired at the end of the experiment at 0.5 V. (Reprinted from Reference 72 with permission.)

face platinum atom). In addition to atop coordination, this mode of bonding is also referred to as terminal or linear coordination. The weaker bands at 1850 cm^{-1} and 1773 cm^{-1} indicate the presence of adsorbed CO in two- and three-fold bridging sites, respectively.[21,22,72]

The vibrational band assignments were supported by *in situ* STM measurements on Pt(111)/CO at –0.25 and +0.1 V.[73] The real-space CO adlayer structures are shown in Figure 5. At –0.25 V, the adlayer has a (2 × 2)–3CO structure. The majority of CO molecules occupy threefold bridging sites on the surface, with a bridging-to-atop CO ratio of 2:1. As the infrared spectra suggest,

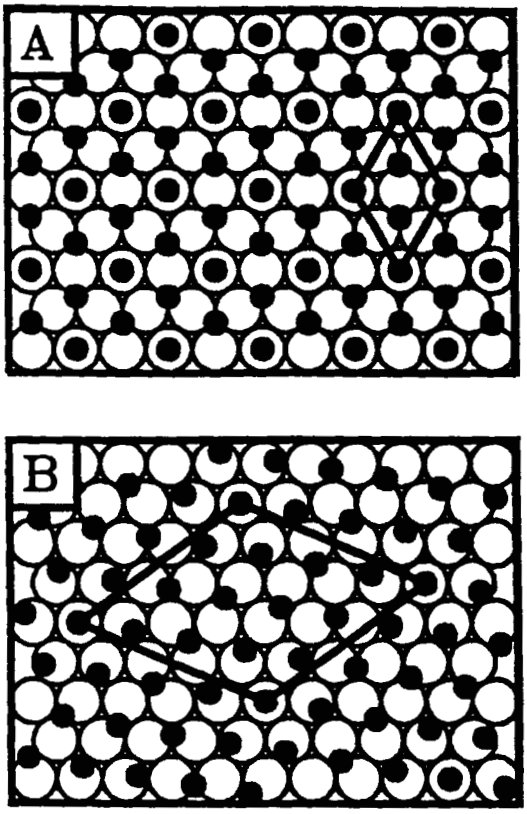

FIGURE 5. Ball models of the real-space structures of the CO adlayers formed on a Pt(111) electrode in CO saturated 0.1 M $HClO_4$ solution by *in situ* STM. (A) The (2 × 2)-3CO structure formed at –0.25 V (vs. SCE). (B) The (√19 × √19)–R23.4° structure formed at +0.1 V (vs. SCE). (Reprinted from Reference 73 with permission.)

the adlayer undergoes a structural transformation at more positive potentials. At +0.1 V, the adlayer adopts a complex (√19 × 19)-R23.4° structure, in which CO occupies atop, twofold bridging and asymmetric sites (sites intermediate between atop and bridging).[72,73]

It has been determined that the shifts in CO site occupancy are driven by changes in the electrode surface potential.[72,73,75,79] Bridge bonding relieves metal-d$\pi \rightarrow$CO-2π^* backbonding, which increases as the potential shifts negative.[2,79] These transformations were first detected with infrared spectroscopy,[2,80] and later confirmed by *in situ* STM.[72,73,75] The shifts are strongest at low CO surface coverages[69] and high negative potentials.[79] More striking potential induced adlayer structural changes have been observed for CO on Rh(111). The CO adlayer on Rh(111) can undergo a nearly complete conversion from atop to twofold bridging within a potential range of less than 1 V.[75]

The *in situ* STM results for Pt(111)/CO raised the issue of why if the majority of CO molecules occupy bridging sites are the atop CO bands in Figure 4 so much more intense than the bridging CO features.[72] Subsequent studies showed that at least part of the intensity disparity is due to interactions between neighboring adsorbates.[73] As discussed in detail below, these effects have great significance for the detection and quantification of adsorbates at different sites on surfaces.

2. Adlayer Intermolecular Coupling Effects on Vibrational Spectra

Adsorbate intermolecular coupling has been recognized as important since the early infrared spectroscopy studies of molecular adsorption on metal catalyst particles.[81,82] In this initial work, the atop CO stretching vibrational bands shifted to lower energy with decreasing CO surface coverages on platinum catalysts.[82] In addition, when catalysts were dosed with mixtures of ^{12}CO and ^{13}CO, the intensities of the atop CO vibrational

bands did not reflect the isotope composition in the adlayer. The ratio of ^{12}CO to ^{13}CO band intensities was greater than the relative surface coverages of these isotopes.[81,82] It was shown that the spectral perturbations could arise from interactions between the transition dipole moments of neighboring adsorbates (dipole-dipole coupling). The spectra were modeled successfully by classic vibrational theory, using the potential function for the coupling of point dipoles to compute the interaction force constants.[82]

Since the early work with catalysts, coupling among adsorbates has been studied under a variety of conditions at both gas/solid (cf. References 3,21–23,83) and liquid/solid interfaces (cf. References 2,52,53,68, 71,72,84–88). Coupling has been observed most often, but not exclusively, for adsorbed CO (cf. References 3,21–23). It is detected primarily as a shift to higher energy of the C-O stretching vibrational modes with increasing CO surface coverage. However, band intensity disparities also occur. For related vibrational modes of molecules at different structural sites, or molecules with different atomic masses bonded to similar surface sites, the band intensities do not reflect the coverage of each species in the adlayer. Coupling is often treated as resulting from purely dipole-dipole forces,[21–23,73,89,90] although through-metal electronic effects are also thought to be important,[91] especially in highly compressed molecular adlayers.[73] The combined effects of dipole-dipole and through-metal and other short-range interactions are referred to as *vibrational coupling*.

Several authors[22,73,83] have used a simple two adsorbate system to demonstrate the physical factors that lead to vibrational coupling-induced frequency shifts and band intensity disparities. For adsorbed CO, two interacting molecules have two C-O stretching vibrational normal modes. When the oscillators are identical (have the same isotopic masses and are adsorbed at symmetrically equivalent sites), the energies of the two modes are degenerate and the bond displacements have the same magnitude in each mode but different phases. The phase of the two oscillators during a vibrational cycle is 0° for one mode and 180° for the other. For each mode, the sum of the bond displacement vectors provides a measure of the total adlayer dipole moment change that occurs during a vibrational cycle, the square of which is proportional to the infrared band intensity (cf. References 22,92,93). In the case of identical oscillators, the in-phase mode has strong infrared absorption, but the out-of-phase mode is infrared inactive, because the C-O stretching displacements add to zero.

When the two interacting CO molecules are bonded to different symmetry sites on the surface or contain different isotopic masses, the vibrational frequencies of the two modes are no longer degenerate and the bond displacement vectors for the two molecules have different magnitudes. The C-O stretching displacements of the high-frequency mode are in-phase, and the mode has strong infrared absorption. The displacement vectors for the lower energy mode are out-of-phase. In this case, the out-of-phase mode is infrared active because the bond displacement vectors for the two oscillators are not equal and therefore do not add to zero. However, the absorption intensity is less for the lower than the higher-energy mode. The intensity disparity increases as the interaction forces become stronger.[22,91]

It has been shown that vibrational coupling between atop and bridging CO molecules is partly responsible for the small bridging-to-atop CO band intensity ratios in Figure 4.[73] Related effects are observed with mixtures of two different CO isotopes (see Section III.A.3), and for CO adsorbed at different structural sites such as steps and terraces (see Section III.A.4). When the coupled oscillator model is applied to larger systems, it becomes apparent that the C-O stretching vibrational bands shift to higher

energy with increasing CO surface coverage because the highest energy states of related vibrational modes have the largest bond displacement vector sums.[22]

Theoretical studies have advanced understanding of the physical and chemical factors that underlie perturbations in spectra of molecular adlayers.[21-23] Approaches have been based on classical vibrational analysis and have differed in the treatment of interaction force constants.[3,21-23] Point dipole approximations have been applied in most models, and image effects have been included to various extents.[3,21-23,73,89] Although the majority of theoretical work has dealt with adsorption at gas/single crystal metal interfaces,[3,21-23,73,89] it has been possible to apply these methods to liquid/single crystal metal interfaces in part with knowledge of adlayer structures from *in situ* STM.[72,73]

The determination of interaction force constants has been aided by vibrational spectra of adlayers that contain mixtures of ^{12}CO and ^{13}CO isotopes. Parameters in the dipole-coupling and short-range interaction terms of the adlayer force field have been derived from numerical fits to mixed isotope spectra (cf. References 21–23,73,82,89,94–97). These experiments and their use in electrochemistry are described below.

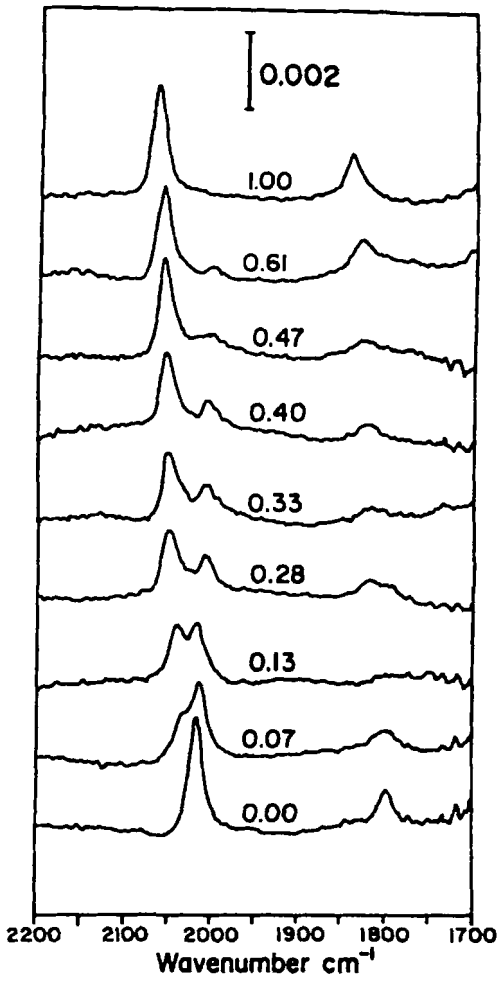

FIGURE 6. Infrared spectra for mixtures of ^{12}CO and ^{13}CO on a Pt(111) electrode at +0.1 V vs. SCE. The numbers above each spectrum are the $^{12}CO/^{13}CO$ fraction. All other parameters are the same as Figure 4. (Reprinted from Reference 73 with permission.)

3. Isotope Mixture Experiments

Addition of a second isotope to an adlayer lowers the symmetry and leads to new infrared active vibrational modes. Comparing the positions and relative intensities of bands for related modes of different isotopes provides information about the adlayer force field. Similar to the theory of vibrational coupling, isotope mixture experiments have evolved through studies of adsorption at gas/solid interfaces, but have also been used to probe electrochemical interfaces (cf. References 68,71,73,84,85,93).

Figure 6 shows infrared spectra of $^{12}CO/^{13}CO$ mixtures at saturation coverage on a Pt(111) electrode at +0.1 V. The atop CO bands appear in the range 2000 to 2100 cm^{-1}. For $^{12}CO/^{13}CO$ fractions between 0.07 to 0.61, separate atop CO bands associated with modes of the different isotopes are observed. The bands at high and low energy are due to vibrational modes that involve C-O stretching motion of mainly atop ^{12}CO and ^{13}CO, respectively. The band intensities show effects of intermolecular coupling. The atop CO high- to low-energy band intensity ratio in each spectrum is greater than expected based on the isotope composition of

the adlayer. For example, at a $^{12}CO/^{13}CO$ isotope fraction of 0.47, the atop ^{12}CO band is much stronger than the atop ^{13}CO band. In the absence of coupling, the intensities would be nearly equal and would reflect the approximately 50:50 mix of the two isotopes in the adlayer. Due to intermolecular coupling, this latter condition is only fulfilled at much lower $^{12}CO/^{13}CO$ fractions, near 0.13.

Figure 7 shows simulated spectra for a saturated CO adlayer on a Pt(111) electrode at +0.1 V.[73] The spectra were computed assuming the molecules interacted only through dipole-dipole forces and the adlayer adopted the $(\sqrt{19} \times \sqrt{19})$-R23.4° structure shown in Figure 5B. Simulations were performed on an array of 300 molecules using periodic boundary conditions to minimize edge effects. The isotopic identity of each molecule was chosen using a random-number generator, and the results were averaged over 100 randomly generated mixtures. Five parameters in the force field were determined through least squares fit to the experimental

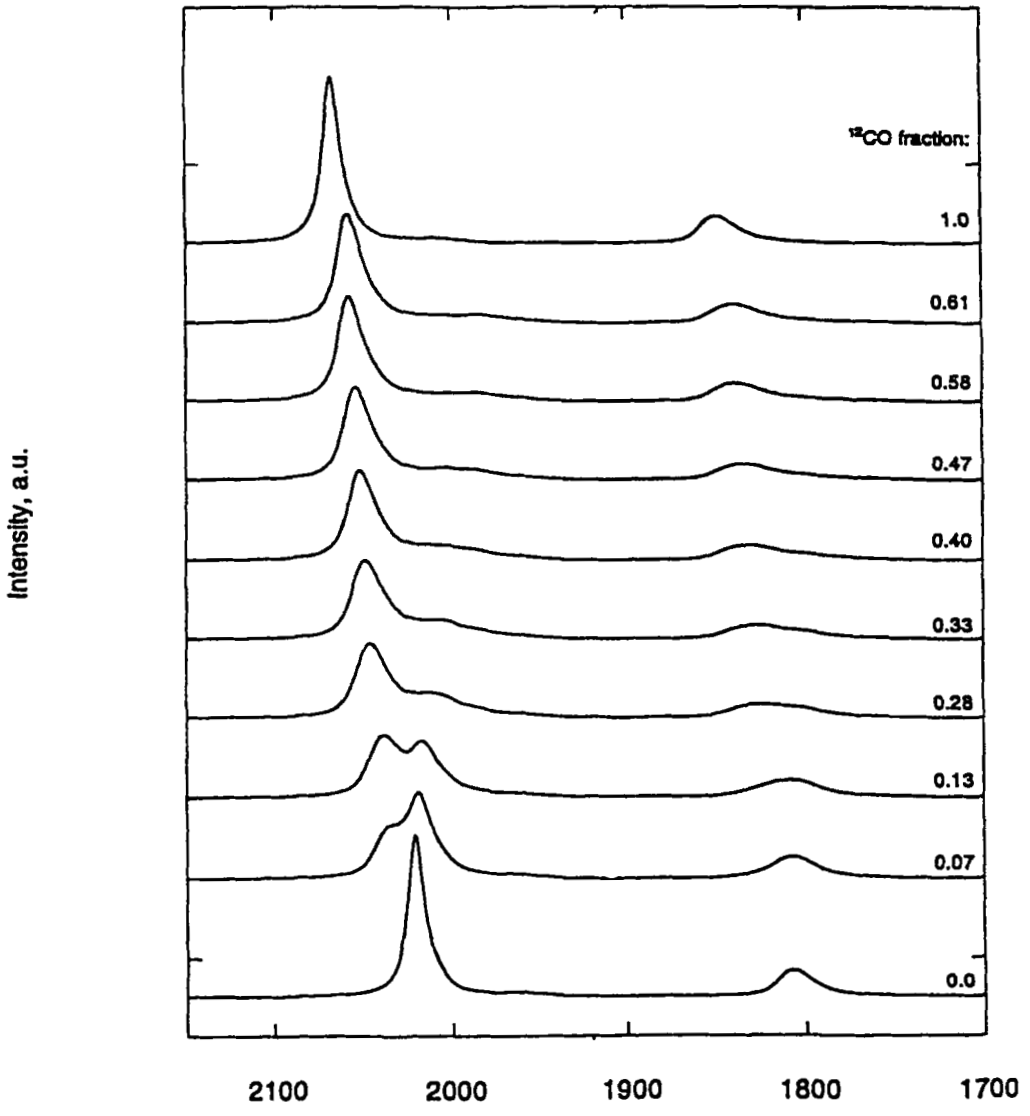

FIGURE 7. Simulated spectra for mixtures of ^{12}CO and ^{13}CO in the $(\sqrt{19} \times \sqrt{19})$–R23.4° structure on Pt(111). (Reprinted from Reference 73 with permission.)

spectra in Figure 6. The best fit parameters were used to compute the spectra in Figure 7. The good agreement between the spectra in Figures 6 and 7 indicates that the intermolecular interactions within the adlayer are dominated by dipole-dipole forces.

When the theoretical treatment was applied to the (2 × 2)-3CO adlayer, dipole-dipole coupling alone was not sufficient to give satisfactory agreement between the experimental and simulated infrared spectra.[73] The interaction potential required an additional term to account for short-range forces between adsorbates. The differences between experiment and pure dipole-dipole coupling theory are thought to result from the unusually high adsorbate packing density in the (2 × 2)-3CO adlayer.[73]

Isotope mixture experiments are also used in a more qualitative fashion to separate dipole-dipole and chemical bonding contributions to coverage dependent vibrational frequency shifts.[21–23] These measurements have allowed assessments of the effects of experimental conditions (e.g. surface structure, adsorbate dosing method) on adsorbate packing density (cf. References 68,71). An application of this approach is discussed in Section III.A.4.

4. Detection of Adsorbates at Different Structural Sites on Surfaces

Infrared spectroscopic detection of molecules adsorbed at different surface structural sites (e.g., steps and terraces) is affected by vibrational coupling. The consequences are apparent in the coverage-dependent spectra of CO adsorbed on a Pt(557) ≡ Pt(s)–[6(111) × (100)] electrode in Figure 8. This surface has 6-atom wide (111) terraces separated by single atom steps of (100) orientation. On stepped platinum surfaces at ambient temperatures, CO preferentially binds to the low coordination step sites and occupies the terraces after the steps essentially fill.[98–100] The spectrum recorded for CO at 16% of saturation (θ/θ_{max} = 0.16) shows C-O stretching vibrational features for CO in atop and bridging coordination environments (ca. 2020 cm^{-1} and 1800 cm^{-1}, respectively) along the steps. The high-energy shoulder on the ca. 1800 cm^{-1} band is possibly due to some bridging CO on the terraces. The start of atop CO occupation of the terraces is signaled by a splitting in the atop CO band, as in the θ/θ_{max} = 0.49 spectrum. The higher-energy feature in the pair grows as the CO coverage increases between θ/θ_{max} = 0.5 to 1.0. However, near saturation only one atop and one bridging CO vibrational band appears, even though for each coordination environment CO occupies both steps and terraces.

The coverage dependence of CO vibrational features on stepped platinum surfaces has been studied in-depth in electrochemical[69–71,88] and uhv[92,98,101–108] environments. The band shifts and intensity disparities are a consequence of vibrational coupling between molecules on steps and terraces. Because the dipole-dipole forces scale as d^{-3},[73,89,92,103] where d is the distance between molecules, these interactions tend to increase with coverage and cause intensity to shift into the highest energy bands of related modes. Near saturation, only single bands for the atop and bridging species appear due to strong coupling and high two-dimensional order in the adlayer.

Intermolecular coupling has been investigated with $^{12}CO/^{13}CO$ mixtures on Pt(335) ≡ Pt(s)–[4(111) × (100)] and Pt(111) electrodes.[71] Values for the dipole-shift, which is the vibrational frequency shift that arises from dipole-dipole coupling (cf. References 21–23,71), were measured for atop CO as a function of surface coverage. Dipole-shift values were determined from $^{12}CO/^{13}CO$ mixtures at constant CO coverages. The values are computed by taking the difference between the atop ^{12}CO band fre-

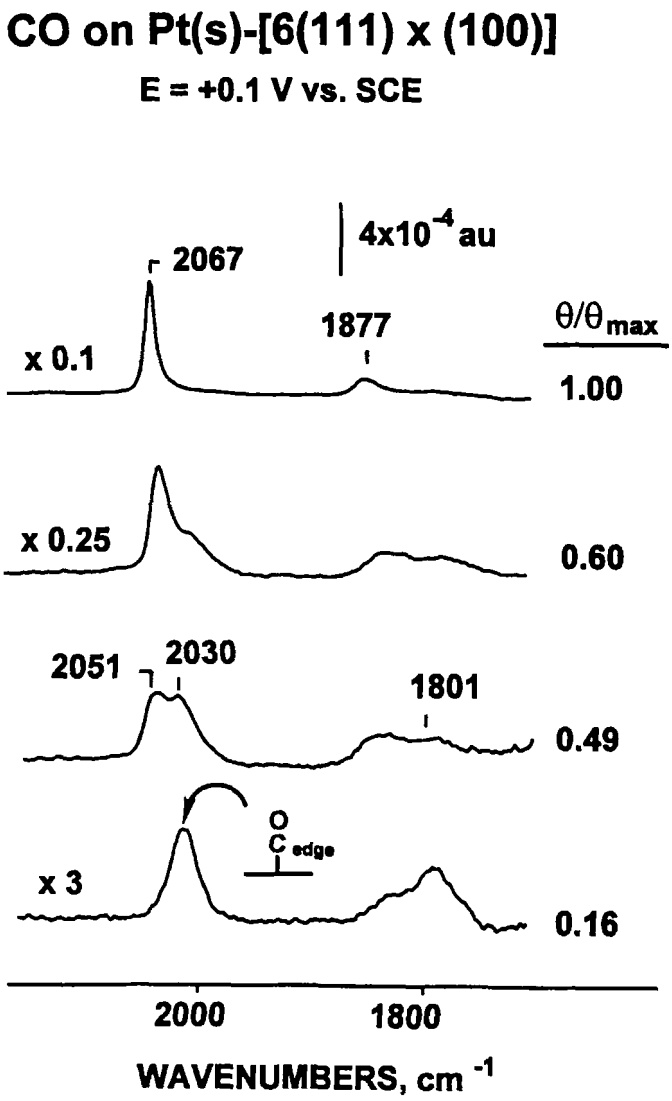

FIGURE 8. Spectra of CO adsorbed at different coverages on a Pt(s)-[6(111) x (100)] electrode maintained at a potential of 0.1 V (vs. SCE) in 0.1 *M* $HClO_4$. The surface coverages are expressed as a fraction of saturation (θ/θ_{max}). (Adapted from Reference 88 with permission.)

quency at an adlayer composition of 100% ^{12}CO and the atop ^{12}CO band frequency in the limit of zero $^{12}CO/^{13}CO$ fraction.[21–23] The latter can be determined from a plot of atop ^{12}CO frequency vs. $^{12}CO/^{13}CO$ fraction by extrapolation (see Reference 71, and references therein).

The dipole shift values measured for CO on Pt(111) and Pt(335) electrodes at +0.1 V (vs. SCE) are plotted vs. the CO surface coverage in Figure 9. For both surfaces the dipole-shift is weak at low coverages. On Pt(111), the dipole-coupling increases fairly uniformly with coverage, reflecting the regu-

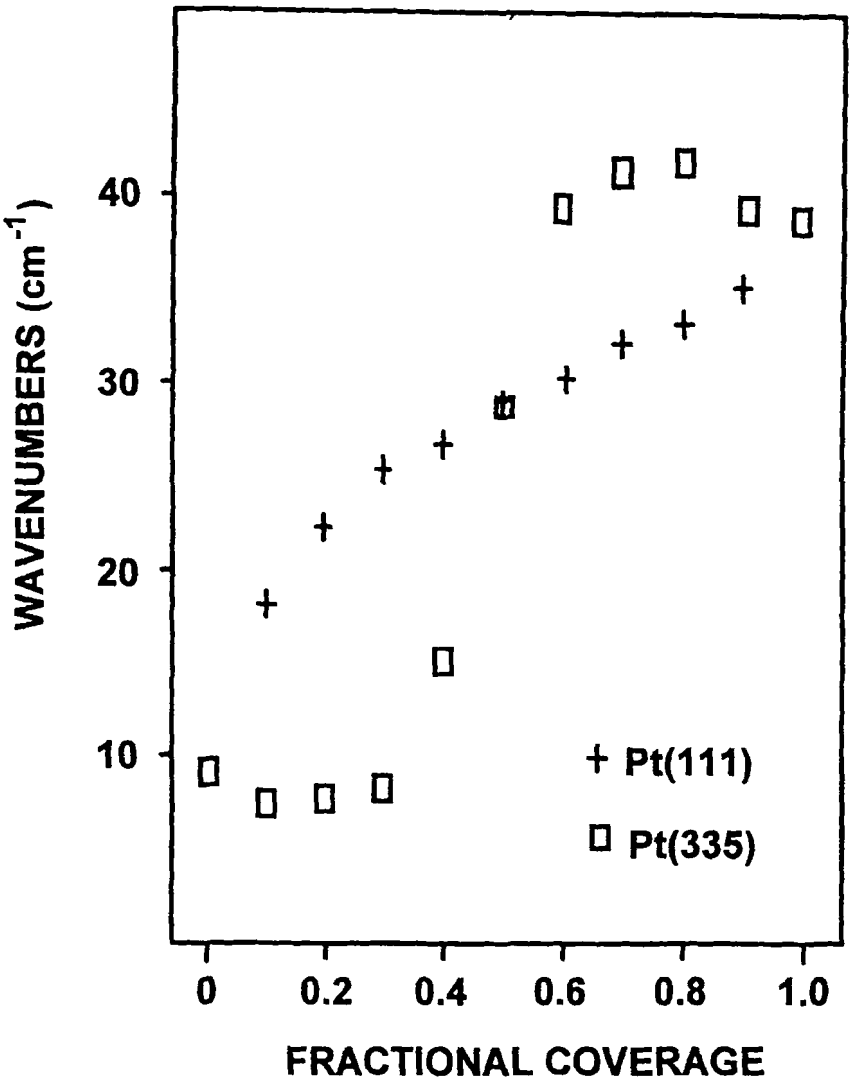

FIGURE 9. Plot of the dipole-shift vs. fractional CO coverage on Pt(111) and Pt(335) ≡ Pt(s)–[4(111) × (100)] electrodes. The dipole-shift values were obtained from infrared spectra of $^{12}CO/^{13}CO$ mixtures with the electrodes at +0.1 V (vs. SCE) in 0.1 *M* $HClO_4$. (Adapted from Reference 71 with permission.)

lar, two-dimensional growth of the adlayer. On Pt(335), the dipole-shift is nearly constant between 0 to 35% of saturation. The weak coupling results from the preferential occupation of CO along step edges, which confines the strong coupling to the dimension along the steps. The sharp increase in dipole-shift value between 35 to 65% of saturation is coincident with the occupation of atop CO on the terraces and the growth of the adlayer in two dimensions across the terrace planes. At high coverages, the coupling is stronger on Pt(335) than on Pt(111), likely due to the high CO coverages supported along the steps.[71,99]

5. Dielectric Screening Effects on Vibrational Spectra of Adsorbates

Intermolecular interactions between adsorbed CO and polarizable coadsorbates, such as organic solvents and metal adatoms, also attenuate the intensities of adsorbed CO

vibrational bands.[78,109–111] This effect and its relevance to *in situ* infrared spectra of electrochemical interfaces was demonstrated recently for coadsorption of CO and common organic solvents on Pt(111) in uhv.[78] For low CO dosages, the C-O stretching band intensities diminished after exposure to nonaqueous solvents and did not reflect the CO surface coverage.[78] The intensity depressions were believed to be caused by screening of the CO dipole local electric fields by the polarizable electrons of the organic coadsorbates. The intensity effects were only detectable when the CO coverages were low enough to allow the coadsorption of the organic solvents.

Due to dielectric screening, it has been difficult to detect CO on electrodes for coverages below saturation in nonaqueous solvents, such as acetonitrile.[78] In contrast, CO has been detected readily down to ~0.1 monolayer in aqueous electrolytes. It appears that, compared with water, the approximately three times larger acetonitrile electronic polarizability allows more complete screening.[78] As it affects adsorbate band intensities, dielectric screening, which occurs through similar dipole-dipole forces that operate among adsorbed CO molecules, is an important consideration for interpretation of *in situ* infrared spectra of electrochemical interfaces.

B. Polarization Modulation Infrared Spectroscopy with Real-Time Sampling Electronics

Experimental techniques for *in situ* infrared detection of electrochemical species have been in use for almost 2 decades and continue to undergo improvement with advances in instrumentation. Developments in polarization modulation spectroscopy have occurred recently with the introduction of high-speed sampling electronics. The configuration for the signal processing electronics used with this technique are included in the optical layout for polarization modulation infrared reflectance spectroscopy in Figure 1B. The electronics sample the interferogram and compute average (I_A) and difference (I_D) signals in real-time. This arrangement overcomes bandwidth limitations of traditional polarization modulation FTIR spectroscopy methods that employ a lock-in amplifier for detector signal demodulation. For example, modern FTIR spectrometers using mercury cadmium telluride (MCT) detectors modulate the mid-infrared wavelengths at frequencies well above the low-pass filter cutoff of the lock-in amplifier output electronics (cf. References 25,26). To prevent attenuation of the high wavenumber optical signals, mirror velocities are lowered, but at the expense of detector response, interferometer stability, and signal averaging capability. The digital electronics allow sampling at rates above the PEM modulation frequency (typically 74 kHz), enabling the mirror to be run at normal velocity. Figure 1B shows the sampling electronics also permit access to the interferogram from the parallel polarized reflectance signal (I_P).

Faguy and co-workers have applied the real-time polarization modulation (RTPM) technique to investigate adsorption at electrochemical interfaces.[24,55] RTPM showed excellent rejection of signals common to both p- and s-polarized radiation states. Compared with SLP measurements, RTPM spectra contained fewer atmospheric and bulk solution interferences and improved detection in the water bending and O-H stretching spectral regions.[24,55] With a combination of SLP and RTPM measurements, better discrimination between surface, bulk solution, and diffuse layer effects was possible.

In addition to improvements in interferogram sampling, enhancements in the optical layout and spectral processing routines accompanied the development of the real-time electronics.[25,26] The zinc selenide lens that replaces the detector focusing mirror reduces polarization phase shifts after

the electrode. It has also been possible to remove the wavelength-dependent response of the PEM from reflectance spectra mathematically rather than through subtraction of a separate background spectrum.[25,26] However, the latter advance has been most useful for the acquisition of spectra from thin films on metals in air rather than species on electrodes.[25] RTPM will likely replace lock-in amplifier-based polarization modulation techniques in electrochemistry as it gains more widespread use.

C. Step-Scan FTIR Spectroscopy in Electrochemistry

An emerging technique for the collection of *in situ* spectra of electrochemical interfaces is step-scan FTIR spectroscopy (cf. Reference 43). This approach combines the noise reduction advantages of potential modulation with the throughput and signal averaging capabilities of FTIR spectroscopy. The step-scan method as applied to electrochemistry is in its initial stages of development. So far, its use has been demonstrated mainly through studies of the archetypal Pt/CO system.

Figure 10 shows a block diagram of an experimental set up for performing EMIRS measurements (Section II.C) with a step-scan FTIR spectrometer. In this arrangement, the electrochemical cell potential is continuously modulated at about 5 to 20 Hz during the collection of an interferogram. With the step-scan instrument, the interferogram is recorded as the optical path in the interferometer is changed incrementally rather than continuously as in a conventional rapid scanning instrument. Further, the adaptation in Figure 10 illustrates the use of the spectrometer in phase modulation mode. In this case, the fixed mirror is dithered sinusoidally (ca. 400 Hz) between steps to produce a high-frequency modula-

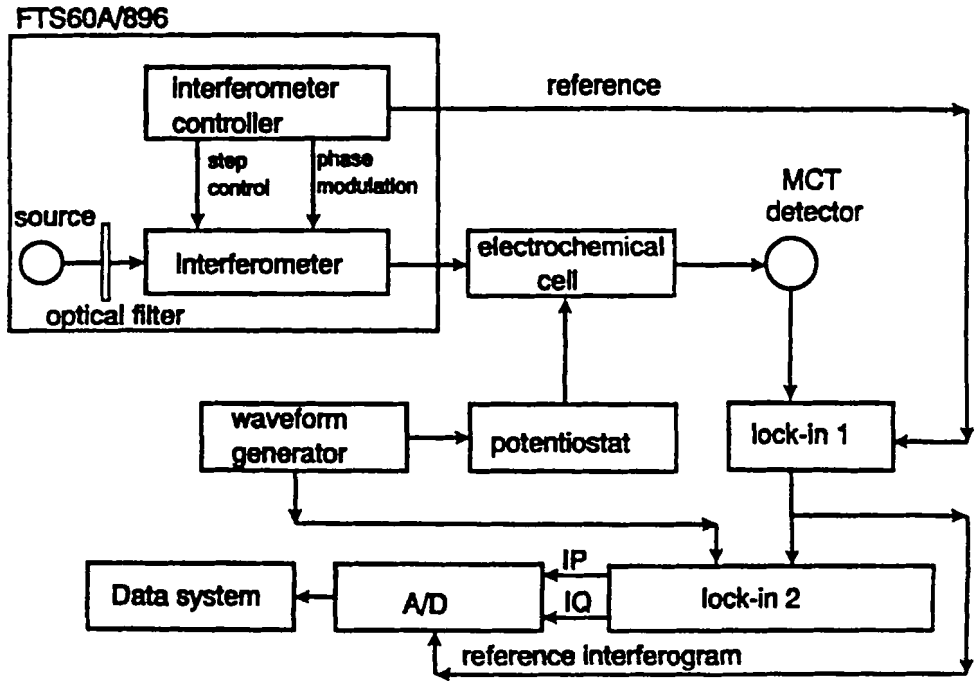

FIGURE 10. Block diagram of the experimental arrangement for potential modulation measurements using a phase-modulated step-scan FTIR spectrometer. (Reprinted from Reference 43 with permission.)

tion in the detector signal, which is recovered with the first lock-in amplifier. Step-scan interferograms can be recorded without phase modulation; however, in electrochemical experiments the use of phase modulation has improved the signal-to-noise ratio by about a factor of 10.[43]

Inasmuch as the first lock-in amplifier is referenced to the 400-Hz mirror dither frequency, and the time constant is kept short (~40 ms), the output still carries the low-frequency signal induced by the electrochemical cell potential modulation. Therefore, the output of the first lock-in amplifier is fed into the second lock-in amplifier to recover the changes induced in the detector signal by the electrode potential modulation. After a settling period, the in-phase and quadrature outputs of the second lock-in amplifier and the electromodulated signal from the first lock-in amplifier are digitized and stored. The data acquisition process is repeated at every step of the moving mirror. An interferogram from each of the three signals (in-phase, quadrature, and electromodulated reference) can be reconstructed from the stored data at the end of a complete mirror scan.

The use of step-scan FTIR spectroscopy in electrochemistry has been demonstrated through studies of CO adsorption on polycrystalline platinum.[43] This system has served as a model for identifying optimum data acquisition parameters and solving problems associated with the mathematical phase correction of the differential interferograms that result from these modulation experiments.[43] In addition to their structural content, step-scan FTIR spectra also provide time-dependent information about electrochemical processes. Having access to both in-phase and quadrature spectra permits identification of those species that follow the potential modulation and those that lag behind. Measurement of spectra as a function of the potential modulation frequency can be useful for the study of periodic events.

IV. CONCLUSIONS

Infrared spectroscopy is an important structural tool for the study of electrochemical interfaces and the identification of solution phase species involved in electrochemical processes. This review has focused on recent advances in instrumentation and methods for CO adlayer characterization. Physical effects that limit detection of adsorbates, such as dipole-dipole coupling and dielectric screening, have been emphasized. The aim has been to concentrate on important analytical factors that have general relevance for infrared spectroscopic studies in electrochemistry. Several other areas of application have not been covered. Some of these include the detection of adsorbed supporting electrolyte ions[16] and organic molecules,[11,17,112] uhv modeling of electrochemical double-layers,[17] and organic oxidation reactions.[1] An effort has been made to cite references to reviews in these areas throughout the text.

ACKNOWLEDGMENT

I wish to thank Prof. M. W. Severson (Oakland University) for many valuable discussions during the past several years of vibrational coupling and related phenomena. Thanks are also extended to Prof. M. J. Weaver (Purdue University) for providing a preprint of Reference 17. Support for our work in this area by the Office of Naval Research is gratefully acknowledged.

REFERENCES

1. Beden, B.; Leger, J.-M.; Lamy, C., *Modern Aspects of Electrochemistry*; Bockris, J. O. M., Conway, B. E. and White, R. E., Ed.; Plenum: New York, 1992; Vol. 22, pp. 97.
2. Chang, S. C.; Weaver, M. J. *J. Phys. Chem.* **1991**, *95*, 5391.

3. Korzeniewski, C.; Severson, M. W. *Spectrochim. Acta* **1995**, *51A*, 499.

4. Fan, Q.; Pu, C.; Smotkin, E. S. *J. Electrochem. Soc.* **1996**, *143*, 3053.

5. Bewick, A.; Pons, B. S., *Advances in Infrared and Raman Spectroscopy*; Clark, R. J. H. and Hester, R. E., Ed.; Wiley: London, 1985; Vol. 12, pp. 1.

6. Pons, S.; Foley, J. K.; Russell, J.; Severson, M., *Modern Aspects of Electrochemistry*; Bockris, J. O. M., Conway, B. E., and White, R. E., Ed.; Plenum Press: New York, 1986; Vol. 17, pp. 223.

7. Foley, J.; Korzeniewski, C.; Daschbach, J. L.; Pons, S., *Electroanalytical Chemistry*; Bard, A. J., Ed.; Marcel Dekker: New York, 1986; Vol. 14, pp. 309.

8. Korzeniewski, C.; Pons, S. *Prog. Analyt. Spectrosc.* **1987**, *10*, 1.

9. Beden, B.; Lamy, C., *Spectroelectrochemistry: Theory and Practice*; Gale, R. J., Ed.; Plenum Press: New York, 1988, pp. 189.

10. Ashley, K.; Pons, B. S. *Chem. Rev.* **1988**, *88*, 673.

11. Stole, S. M.; Popenoe, D. D.; Porter, M. D., *Electrochemical Interfaces. Modern Techniques for In-Situ Interface Characterization*; Abruna, H. D., Ed.; VCH Publishers, Inc.: New York, 1991, pp. 339.

12. Iwasita, T; Nart, F. C. *Advances in Electrochemical Science and Engineering;* Gerischer, H.; Tobias, C. W., Eds.; VCH Publishers, Inc.: New York, 1991. Vol. 4, pp. 123.

13. Ashley, K. *Talanta* **1991**, *38*, 1209; *Spectroscopy* **1990**, *5*, 22.

14. Chang, S. C.; Hamelin, A.; Weaver, M. J. *J. Chim. Phys.* **1991**, *86*, 1615.

15. Weaver, M. J. *Appl. Surf. Sci.* **1993**, *67*, 147.

16. See reviews in *Electrochim. Acta. (Special Edition)*; Iwasita, T., Ed., 1996; Vol. 41.

17. Weaver, M. J.; Zou, S., in *Advances in Spectroscopy*; Clark, R. J. H. and Hester, R. E., Ed.; Wiley: New York, 1997; Vol. 26 (submitted).

18. Porter, M. D. *Anal. Chem.* **1988**, *60*, 1143A.

19. Greenler, R. G. *J. Chem. Phys.* **1966**, *44*, 310.

20. Greenler, R. G. *J. Chem. Phys.* **1969**, *50*, 1963.

21. Hayden, B. E., *Vibrational Spectroscopy of Molecules on Surfaces*; Yates, J. T., Jr. and Madey, T. E., Ed.; Plenum Press: New York, 1987; Vol. 1, pp. 267.

22. Hollins, P.; Pritchard, J. *Progr. Surface Sci.* **1985**, *19*, 275.

23. Willis, R. F.; Lucas, A. A.; Mahan, G. D., *The Chemical Physics of Solid Surfaces and Heterogeneous Catalysis*; King, D. A. and Woodruff, D. P., Ed.; Elsevier: Amsterdam, 1983; Vol. 2, pp. 59.

24. Richmond, W. N.; Faguy, P. W.; Jackson, R. S.; Weibel, S. C. *Anal. Chem.* **1996**, *68*, 621.

25. Barner, B. J.; Green, M. J.; Saez, E. I.; Corn, R. M. *Anal. Chem.* **1991**, *63*, 55.

26. Green, M. J.; Barner, B. J.; Corn, R. M. *Rev. Sci. Instrum.* **1991**, *62*, 1426.

27. Bae, I. T.; Sandifer, M.; Lee, Y. W.; Tryk, D. A.; Sukenik, C. N.; Scherson, D. A. *Anal. Chem.* **1995**, *67*, 4508.

28. Parry, D. B.; Harris, J. M.; Ashley, K. *Langmuir* **1990**, *6*, 209.

29. Neugebauer, H.; Nauer, G.; Brinda-Konopik, N.; Gidaly, G. *J. Electroanal. Chem.* **1981**, *122*, 381.

30. Pham, M.-C.; Lacaze, P.-C. *J. Electrochem. Soc.* **1994**, *141*, 156.

31. Harrick, N. *Internal Reflection Spectroscopy*; Interscience Publishers: New York, 1967.

32. Corrigan, D. S.; Weaver, M. J. *J. Electroanal. Chem.* **1988**, *239*, 55.

33. Bae, I. T.; Xing, X.; Yeager, E. B.; Scherson, D. *Anal. Chem.* **1989**, *61*, 1164.

34. Bae, I. T.; Scherson, D. A.; Yeager, E. B. *Anal. Chem.* **1990**, *62*, 45.

35. Roth, J. D.; Weaver, M. J. *Anal. Chem.* **1991**, *63*, 1603.

36. Sundholm, G.; Talonen, P. *J. Electroanal. Chem.* **1994**, *377*, 91.

37. Seki, H.; Kunimatsu, K.; Golden, W. G. *Appl. Spectrosc.* **1985**, *39*, 437.

38. Popenoe, D. D.; Stole, S. M.; Porter, M. D. *Appl. Spectrosc.* **1992**, *46*, 79.

39. Faguy, P. W.; Marinkovic, N. S. *Appl. Spectrosc.* **1996**, *50*, 394.

40. Roe, D. K.; Sass, J. K.; Bethune, D. S.; Luntz, A. C. *J. Electroanal. Chem.* **1987**, *216*, 293.

41. Faguy, P. W.; Fawcett, W. R. *Appl. Spectrosc.* **1990**, *44*, 1309.

42. Bethune, D. S.; Luntz, A. C.; Sass, J. K.; Roe, D. K. *Surf. Sci.* **1988**, *197*, 44.

43. Budevska, B. O.; Griffiths, P. R. *Anal. Chem.* **1993**, *65*, 2963.

44. Faguy, P. W.; Marinkovic, N. S. *Anal. Chem.* **1995**, *67*, 2791.

45. Corrigan, D. S.; Leung, L. W. H.; Weaver, M. J. *Anal. Chem.* **1987**, *59*, 2252.

46. Leung, L. W. H.; Weaver, M. J. *Langmuir* **1990**, *6*, 323.

47. Beden, B.; Lamy, C.; Bewick, A.; Kunimatsu, K. *J. Electroanal. Chem.* **1981**, *121*, 343.

48. Golden, W. G., *Fourier Transform Infrared Spectroscopy*; Ferraro, J. R. and Basile, L. J., Ed.; Academic Press: New York, 1985; Vol. 4.

49. Russell, J. W.; Overend, J.; Scanlon, K.; Severson, M.; Bewick, A. *J. Phys. Chem.* **1982**, *86*, 3066.

50. Russell, J. W.; Severson, M.; Scanlon, K.; Overend, J.; Bewick, A. *J. Phys. Chem.* **1983**, *87*, 293.

51. Golden, W. G.; Kunimatsu, K.; Seki, H. *J. Phys. Chem.* **1984**, *88*, 1275.

52. Kunimatsu, K.; Golden, W. G.; Seki, H.; Philpott, M. R. *Langmuir* **1985**, *1*, 245.

53. Kunimatsu, K.; Seki, H.; Golden, W. G.; II, J. G. G.; Philpott, M. R. *Langmuir* **1986**, *2*, 464.

54. Saez, E. I.; Corn, R. M. *Electrochim. Acta* **1993**, *38*, 1619.

55. Faguy, P. W.; Richmond, W. N. *J. Electroanal. Chem.* **1996**, *410*, 109.

56. Clavilier, J.; Faure, R.; Guinet, G.; Durand, R. *J. Electroanal. Chem.* **1980**, *107*, 205.

57. Clavilier, J. *J. Electroanal. Chem.* **1980**, *107*, 211.

58. Clavilier, J.; Durand, R.; Guinet, G.; Faure, R. *J. Electroanal. Chem.* **1981**, *127*, 281.

59. Wagner, F. T.; P.N. Ross, J. *J. Electroanal. Chem.* **1983**, *150*, 141.

60. Hamelin, A., *Mod. Aspects Electrochem*; White, R. E., Bockris, J. O. M. and Conway, B. E., Ed.; Plenum Press: New York, 1985; Vol. 16, pp. 1.

61. Clavilier, J., *Electrochemical Surface Science*; Soriaga, M. P., Ed.; American Chemical Society: Washington, D.C., 1988; Vol. 378, pp. 14.

62. Zurawski, D.; Rice, L.; Hourani, M.; Wieckowski, A. *J. Electroanal. Chem.* **1987**, *230*, 221.

63. Hourani, M.; Wieckowski, A. *J. Electroanal. Chem.* **1987**, *227*, 259.

64. Wasberg, M.; Palaikis, L.; Wallen, S.; Kamrath, M.; Wieckowski, A. *J. Electroanal. Chem.* **1988**, *256*, 51.

65. Chang, S. C.; Leung, L. W. H.; Weaver, M. J. *J. Phys. Chem.* **1990**, *94*, 6013.

66. Edens, G. J.; Gao, X.; Weaver, M. J. *J. Electroanal. Chem.* **1994**, *375*, 357.

67. Marinkovic, N. S.; Calvene, J. J.; Kovacova, Z.; Fawcett, W. R. *J. Electrochem. Soc.* **1996**, *143*, L171.

68. Chang, S. C.; Weaver, M. J. *J. Chem. Phys.* **1990**, *92*, 4582.

69. Kim, C. S.; Tornquist, W. J.; Korzeniewski, C. *J. Phys. Chem.* **1993**, *97*, 6484.

70. Kim, C. S.; Korzeniewski, C.; Tornquist, W. J. *J. Chem. Phys.* **1994**, *100*, 628.

71. Kim, C. S.; Tornquist, W. J.; Korzeniewski, C. *J. Chem. Phys.* **1994**, *101*, 9113.

72. Villigas, I.; Weaver, M. J. *J. Chem. Phys.* **1994**, *101*, 1648.

73. Severson, M. W.; Stuhlmann, C.; Villegas, I.; Weaver, M. J. *J. Chem. Phys.* **1995**, *103*, 9832.

74. Stuhlmann, C.; Villegas, I.; Weaver, M. J. *Chem. Phys. Lett.* **1994**, *219*, 319.

75. Yau, S. L.; Gao, X.; Chang, S. C.; Schardt, B. C.; Weaver, M. J. *J. Am. Chem. Soc.* **1991**, *113*, 6049.

76. Gao, X.; Chang, S. C.; Jiang, X.; Hamelin, A.; Weaver, M. J. *J. Vac. Sci. Technol., A* **1992**, *10*, 2972.

77. Weaver, M. J.; Gao, X. *Annu. Rev. Phys. Chem.* **1993**, *44*, 459.

78. Kizhakevariam, N.; Villegas, I.; Weaver, M. J. *Langmuir* **1995**, *11*, 2777.

79. Roth, J. D.; Chang, S.-C.; Weaver, M. J. *J. Electroanal. Chem.* **1990**, *288*, 285.

80. Kitamura, F.; Takahashi, M.; Ito, M. *J. Phys. Chem.* **1988**, *92*, 3320.

81. Eischens, R. P.; Francis, S. A.; Pliskin, W. A. *J. Phys. Chem.* **1956**, *60*, 194.

82. Hammaker, R. M.; Francis, S. A.; Eischens, R. P. *Spectrochim. Acta* **1965**, *21*, 1295.

83. Paul, D. K.; Beebe, T. P., Jr.; Uram, K. J.; Yates, J. T., Jr. *J. Am. Chem. Soc.* **1992**, *114*, 1949.

84. Kunimatsu, K.; Seki, H.; Golden, W. G.; Gordon, J. G., II; Philpott, M. R. *Langmuir* **1988**, *4*, 337.

85. Gao, P.; Weaver, M. J. *J. Phys. Chem.* **1989**, *93*, 6205.

86. Chang, S.-C.; Leung, L.-W. H.; Weaver, M. J. *J. Phys. Chem.* **1989**, *93*, 5341.

87. Chang, S. C.; Roth, J. D.; Weaver, M. J. *Surf. Sci.* **1991**, *244*, 113.

88. Kim, C. S.; Korzeniewski, C. *Anal. Chem.* **1997** *(in press)*.

89. Persson, B. N. J.; Ryberg, R. *Phys. Rev. B* **1981**, *24*, 6954.

90. Persson, B. N. J.; Liebsch, A. *Surf. Sci.* **1981**, *110*, 356.

91. Moskovits, M.; Hulse, J. E. *Surf. Sci.* **1978**, *78*, 397.

92. Leibsle, F. M.; Sorbello, R. S.; Greenler, R. G. *Surf. Sci.* **1987**, *179*, 101.

93. Severson, M. W.; Russell, A.; Campbell, D.; Russell, J. W. *Langmuir* **1987**, *3*, 202.

94. Crossley, A.; King, D. A. *Surf. Sci.* **1977**, *68*, 528.

95. Crossley, A.; King, D. A. *Surf. Sci.* **1980**, *95*, 131.

96. Schweizer, E.; Persson, B. N. J.; Tushaus, M.; Hoge, D.; Bradshaw, A. M. *Surf. Sci.* **1989**, *213*, 49.

97. Olsen, C. W.; Masel, R. I. *J. Vac. Sci. Technol. A* **1988**, *6*, 792.

98. Hayden, B. E.; Kretzschmar, K.; Bradshaw, A. M.; Greenler, R. G. *Surf. Sci.* **1985**, *149*, 394.

99. Luo, J. S.; Tobin, R. G.; Lambert, D. K.; Fisher, G. B.; DiMaggio, C. L. *Surf. Sci.* **1992**, *274*, 53.

100. Henderson, M. A.; Szabo, A.; Yates, J. T., Jr. *J. Chem. Phys.* **1989**, *91*, 7245.

101. Greenler, R. G.; Burch, K. D.; Kretzschmar, K.; Klauser, R.; Bradshaw, A. M.; Hayden, B. E. *Surf. Sci.* **1985**, *153*, 338.

102. Brandt, R. K.; Greenler, R. G. *Chem. Phys. Lett.* **1994**, *221*, 219.

103. Greenler, R. G.; Leibsle, F. M.; Sorbello, R. S. *Phys. Rev. B* **1985**, *32*, 8431.

104. Jansch, H. J.; Xu, J.; Yates, J. T., Jr. *J. Chem. Phys.* **1993**, *99*, 721.

105. Xu, J.; Yates, J. T., Jr. *J. Chem. Phys.* **1993**, *99*, 725.

106. Wang, H.; Tobin, R. G.; Lambert, D. K.; Fisher, G. B.; DiMaggio, C. L. *J. Chem. Phys.* **1995**, *103*, 2711.

107. Lambert, D. K.; Tobin, R. G. *Surf. Sci.* **1990**, *232*, 149.

108. Hollins, P. *Surf. Sci. Rep.* **1992**, *16*, 51.

109. Ehlers, D. H.; Esser, A. P.; Spitzer, A.; Luth, H. *Surf. Sci.* **1987**, *191*, 466.

110. Rodriguez, J. A.; Truong, C. M.; Goodman, D. W. *J. Chem. Phys.* **1992**, *96*, 7814.

111. Rodriguez, J. A.; Truong, C. M.; Goodman, D. W. *Surf. Sci.* **1992**, *271*, L331.

112. Anderson, M. R.; Gatin, M. *Langmuir* **1994**, *10*, 1638.